Pair production in low luminosity galactic nuclei

M. Mościbrodzka[1], C. F. Gammie[1,2], J. C. Dolence[2], H. Shiokawa[2]

[1] *Department of Physics, University of Illinois, 1110 West Green Street, Urbana, IL 61801*

[2] *Astronomy Department, University of Illinois, 1002 West Green Street, Urbana, IL 61801*

ABSTRACT

We compute the distribution of pair production by $\gamma\gamma$ collisions in weakly radiative accretion flows around a black hole of mass M and accretion rate $\dot{M}$. We use a flow model drawn from general relativistic magnetohydrodynamic simulations and a Monte Carlo radiation field that assumes the electron distribution function is thermal. We find that: (1) there is a wedge in the $(M, \dot{M})$ plane where the near-empty funnel over the poles of the black hole is populated mainly by pair production in $\gamma\gamma$ collisions; (2) the wedge is bounded at low accretion rate by a region where the pair density implied by the $\gamma\gamma$ production rate falls below the Goldreich-Julian density. (3) the wedge is bounded at high accretion rate by $\dot{M}_{crit}$. For $\dot{M} > \dot{M}_{crit}$ the models are not weakly radiative and our models are inconsistent, but $\gamma\gamma$ collisions likely still dominate; (4) within the wedge the pair production rate density scales as $\sim \dot{M}^6$, declines as radius r^{-6}, and declines away from the equatorial plane. We provide expressions for the pair production rate as a function of $\dot{M}$ and also as a function of the X-ray luminosity L_X and the X-ray spectral index. We finish with a brief discussion of the implications for Sgr A* and M87.

Subject headings: accretion, accretion disks — black hole physics — MHD — radiative transfer — Galaxy: center

1. Introduction

Models of zero-obliquity black hole accretion—in which the accretion flow angular momentum is parallel to the black hole spin—typically exhibit a low density "funnel" over the poles of the black hole. The funnel is empty because the funnel plasma is free to fall into the hole or blow outward to large radius. Magnetic fields do not prevent this: in magnetohydrodynamic (MHD) simulations of funnels in radiatively inefficient accretion flows (RIAFs) the funnel magnetic field runs in a smooth spiral from the event horizon to large radius (De

Villiers et al. 2003; McKinney & Gammie 2004; Komissarov 2005; Hawley & Krolik 2006; Beckwith et al. 2008). And because the field lines do not leave the funnel there is no resupply route from the disk to the funnel.

What process, then, populates the funnel with plasma? And what controls the temperature (or distribution function) of the funnel plasma? These questions bear directly on two interesting problems in black hole jet theory: are jets made of pairs or an electron-ion plasma? And which is more luminous: the base of the jet or the accretion flow? The purpose of this paper is to investigate these questions in the specific context of hot, underluminous accretion flows where nearly *ab initio* models are computationally feasible.

There are several pair creation processes that might populate the funnel with plasma. Plasma close to the event horizon in a RIAF is relativistically hot, and thus can form electron-positron pairs $e^{\pm}$ through particle-particle (ee, ep), particle-photon ($e\gamma$, $p\gamma$), or photon-photon collisions ($\gamma\gamma$). The cross section near the $e^{\pm}$ energy threshold is largest for $\gamma\gamma$ interactions, which have a cross section $\sim \sigma_T \equiv 8\pi r_0^2/3 \approx 6.652\times10^{-25}\,\mathrm{cm}^2$, the Thomson cross section. In the funnel the photon density vastly exceed the particle density, so $\gamma\gamma$ collisions dominate $e^{\pm}$ production (Stepney & Guilbert 1983, Phinney 1983, Phinney 1995, Krolik 1999). Equilibrium pair production by these processes in the context of Advection Dominated Accretion Flows (ADAFs, Narayan & Yi 1994) is discussed in e.g. Kusunose & Mineshige 1996 and Esin 1999; however these works focus on the energetic role of pairs in ADAF disk rather than the population and dynamics of pairs in the funnel.

At densities below the Goldreich-Julian density (Goldreich & Julian 1969), pairs can be created in a pair-photon cascade (Blandford & Znajek 1977; Phinney 1983; Beskin et al. 1992; Hirotani & Okamoto 1998, and recently Vincent & Lebohec 2010). When the density is low the plasma can have $\mathbf{E}\cdot\mathbf{B} \neq 0$, and the electric field can directly accelerate particles to high Lorentz factors. The energetic particles can then Compton upscatter background photons that collide with other background photons and produce a shower of pairs.

In this paper we model production of an $e^{\pm}$ plasma by photon-photon collisions in the funnel above a hot, underluminous accretion disk. At sufficiently low accretion rates $\dot{M}$ ($\lesssim \dot{M}_{crit} \sim 10^{-6} L_{Edd}/(0.1c^2)$, where $L_{Edd} \equiv$ Eddington luminosity) the disk will cool only over timescales much larger than the accretion timescale; it is a RIAF. In this regime the radiative and dynamical evolution are decoupled and it is practical to treat both on a nearly *ab initio* basis. Throughout the range of $\dot{M}$ we consider the funnel pair plasma is tenuous, so pair production will be balanced by advective losses (accretion into the black hole or loss in a wind) rather than by annihilation.

We draw our RIAF model from two and three dimensional general relativistic magne-

tohydrodynamics simulations (GRMHD, using the HARM code, Gammie et al. 2003) of an accreting, magnetized torus with zero cooling. The radiation field is calculated as a post-processing step using a Monte Carlo method (grmonty, Dolence et al. 2009). Finally pair production rates are estimated in a Monte Carlo fashion from snapshots of the radiation field using a procedure that we describe in detail below.

This paper is organized as follows. In § 2 we describe the basic model for accretion flow dynamics and radiative transfer. In § 3 we write down the pair production model and present a test problem for our Monte Carlo scheme. Scaling formulas are presented in § 4. In § 5 we show results of simulations for varying black hole mass and accretion rate. We briefly discuss implications for Sgr A*and M87 in § 6. We summarize in § 7.

2. Accretion flow model

We use a numerical model for the accretion flow and for the radiation field. These nearly *ab initio* models form a numerical laboratory for investigating physical processes near a black hole.

2.1. Dynamical model

We use a relativistic MHD model for the accreting plasma (see e.g., Gammie et al. 2003). The model begins with a hydrodynamic equilibrium thick disk (Fishbone & Moncrief 1976) in orbit around a Kerr black hole. The initial torus is seeded with poloidal, concentric loops of weak magnetic field that is parallel to density contours, and small perturbations are added to the internal energy. The latter seeds the magnetorotational instability and leads to the development of MHD turbulence in the disk and accretion onto the central black hole. We solve the evolution equations until a quasi-equilibrium accretion flow is established, meaning that the large scale structure of the flow is not evolving on the dynamical timescale. Our models describe accretion onto a black hole with $a_* = 0.94$, where $a_* \equiv Jc/GM^2$ and J is the angular momentum of the black hole. Our numerical model covers $40GM/c^2$. Our (untested) hypothesis is that at $r < 15GM/c^2$ the model accurately represent the inner portions of a relaxed accretion flow extending over many decades in radius. Throughout our model we assume the mass of the accretion flow is small compared to M and that the metric is stationary.

A few of the physical assumptions in the GRMHD model are worth stating explicitly.

We use a γ_{ad}-law equation of state

$$p = (\gamma_{ad} - 1)u \tag{1}$$

where $\gamma_{ad} = 13/9$ (appropriate for ion temperature $T_i < m_p c^2/k = 1.1 \times 10^{13} K$ and electron temperature $T_e > m_e c^2/k = 5.9 \times 10^9 K$), $p \equiv$ pressure, and $u \equiv$ internal energy density. We also assume particle number conservation

$$(\rho_0 u^\mu)_{;\mu} = 0, \tag{2}$$

where $\rho_0 \equiv$ rest-mass density and $u^\mu \equiv$ four-velocity, in the dynamical evolution. That is, we do not explicitly allow for pair production in the dynamical model and instead calculate the pair production rate as a post-processing step. Our model is, therefore, consistent only if pair creation is weak enough not to alter the dynamics or energetics.

We evolve the GRMHD equations using the `harm` code (Gammie et al. 2003). `harm` is a conservative scheme that evolves the total energy rather than internal energy of the flow. The MHD equation integration is performed on a uniform grid in modified Kerr-Schild coordinates (Gammie et al. 2003). The coordinates are logarithmic in the Kerr-Schild radius r and nonuniform in Kerr-Schild colatitude θ (Boyer-Lindquist and Kerr-Schild r and θ are identical), concentrating zones toward the midplane of the accretion disk. The Kerr-Schild coordinates are nonsingular on the horizon, so we can extend the numerical grid through the horizon and isolate the inner boundary inside the black hole. The outer boundary uses an outflow condition. Our axisymmetric models have numerical resolution of 256×256, while the 3D run has resolution of $192 \times 192 \times 128$. The details of the numerical method, the initial setup and full discussion of the flow evolution in 2D see Gammie et al. (2003) and McKinney & Gammie (2004). A snapshot of the density, temperature, and magnetic field strength from one of our runs is shown in Figure 1.

2.2. Radiative model

Applications of radiative models to Sgr A* are discussed in Mościbrodzka et al. (2009). In a thermal plasma with $\Theta_e \equiv kT_e/(m_e c^2) > 1$ the ratio (synchrotron / bremsstrahlung) cooling $\sim \Theta_e^2/(\alpha\beta)$, where $\alpha \equiv$ fine structure constant and $\beta \equiv 8\pi p/B^2$. Synchrotron therefore dominates in an energetic sense the direct production of photons in the inner regions of the flow that we model here, where $\Theta_e \sim 1 - 10^2$ and $\beta \sim 10$. Synchrotron emission occurs at a characteristic frequency $\nu_s \sim (eB/(2\pi m_e c))\Theta_e^2$ which is $\ll m_e c^2/h$

for any astrophysically reasonable combination of M and $\dot{M}$. [1]. Potentially pair-producing photons must therefore be produced by Compton scattering, and so our model includes synchrotron emission, absorption, and Compton scattering.

We compute the radiation field using a Monte Carlo general relativistic radiative transfer code `grmonty`(Dolence et al. 2009); here we outline `grmonty`'s most important features. The radiation field is represented by photon packets (photon rays or 'superphotons'). Each superphoton is characterized by the photon weight w = number of physical photons/superphotons, and the wave four-vector k^μ. The superphotons are produced by sampling the emissivity. The wavevector is then transported according to the geodesic equation. Along a geodesic w is decremented to account for synchrotron absorption. Compton scattering is incorporated by sampling scattering events. When a superphoton scatters it is divided into a scattered piece with new wavevector k'^μ and new weight w', and an unscattered piece along the original wavevector with weight $w - w'$. The distribution of scattered k'^μ is consistent with the full Klein-Nishina differential cross section.

We have used a "fast light" approximation in treating the radiative transfer. The data from a single time slice t_n (e.g. $\rho_0(t_n, x^1, x^2, x^3)$) is used to calculate the emergent radiation field as if the data, and therefore photon field, were time-independent. We have checked, via a time-dependent radiative transfer model (Dolence et al. 2010), that this approximation does not introduce significant errors.

2.3. Model scaling

The dynamical models of a nonradiative accretion are scale free but their radiative properties are not. We specify the simulations length unit

$$\mathcal{L} \equiv \frac{GM}{c^2}, \tag{4}$$

[1]For the synchrotron emissivity we use the approximate expression of Leung et al. (2010)

$$j_\nu = \frac{\sqrt{2}\pi e^2 n_e \nu_s}{3cK_2(\Theta_e^{-1})}(X^{1/2} + 2^{11/12}X^{1/6})^2 \exp(-X^{1/3}) \tag{3}$$

where $X = \nu/\nu_s$, $\nu_s = 2/9(eB/2\pi m_e c)\Theta_e^2 \sin\theta$ is the synchrotron frequency, θ is an angle between the magnetic field vector and emitted photon, and K_2 is a modified Bessel function of the second kind. The fractional error for this approximate formula is smaller than 1% for $\Theta_e \geq 1$ (where most of the emission occurs) and increases to 10% and more at low frequencies for $\Theta_e \leq 1$ (where there is very little emission). The synchrotron emissivity function peaks at $\nu \approx 8\nu_s$.

time unit

$$\mathcal{T} \equiv \frac{GM}{c^3}, \tag{5}$$

and mass unit $\mathcal{M}$, which is proportional to the mass accretion rate. M does not set a mass scale because it appears only in the combination GM. Since $\mathcal{M}$ is negligible in comparison to M there is a scale separation between the two masses.

Once M, and therefore $\mathcal{L}$ and $\mathcal{T}$, and $\mathcal{M}$ are set the radiative transfer calculation is well posed. Typically M can be estimated from observation, while $\mathcal{M}$ is set by requiring the model submillimeter flux match observations.

2.4. Model limitations

It is worth pointing out some of our model's limitations. The plasma is treated as a nonradiating ideal fluid. This implies that the electrons and ions have an isotropic, thermal distribution function. The potentially important effects of pressure anisotropy and conduction are therefore negelected (e.g. Sharma et al. 2006, Johnson & Quataert 2007). The radiative effects of a nonthermal component in the distribution function are also neglected. Cooling is also neglected. This is likely to be unimportant in very low accretion rate systems like Sgr A*, but far more important in higher accretion rate systems like M87. The sign of the effect of neglecting cooling is to raise the density and magnetic field strength, if the synchrotron luminosity is held fixed.

3. Pair production

We now consider how the Monte Carlo description of the radiation field can be transformed into an estimate for the pair creation rate.

3.1. Basic equations

For a population of photons with distribution function $dN_\gamma/d^3x d^3k$ (here $d^3k \equiv dk_1 dk_2 dk_3$ and $1, 2, 3$ are the spatial coordinates) the invariant pair production rate per unit volume is

$$\dot{n}_\pm \equiv \frac{1}{\sqrt{-g}} \frac{dN_\pm}{d^3x dt} = \frac{1}{2} \int \frac{d^3k}{\sqrt{-g}k^t} \frac{d^3k'}{\sqrt{-g}k'^t} \frac{dN_\gamma}{d^3x d^3k} \frac{dN_\gamma}{d^3x d^3k'} \epsilon^2_{[CM]} \sigma_{\gamma\gamma} c \tag{6}$$

where g is the determinant of $g_{\mu\nu}$, and the factor of 1/2 prevents double-counting. Here $\sigma_{\gamma\gamma}$ is the cross section for $\gamma + \gamma \to e^+ + e^-$:

$$\frac{\sigma_{\gamma\gamma}}{\sigma_T} = \frac{3}{8\,{\epsilon_{[\mathrm{CM}]}}^6}\left[(2\,{\epsilon_{[\mathrm{CM}]}}^4 + 2\,{\epsilon_{[\mathrm{CM}]}}^2 - 1)\cosh^{-1}\,\epsilon_{[\mathrm{CM}]} - \,\epsilon_{[\mathrm{CM}]}({\epsilon_{[\mathrm{CM}]}}^2 + 1)\sqrt{{\epsilon_{[\mathrm{CM}]}}^2 - 1}\right] \quad (7)$$

(Breit & Wheeler 1936),

$$\epsilon_{[\mathrm{CM}]} = -u_{CM\mu}k^\mu = -u_{CM\mu}k'^\mu = \left(\frac{-k_\mu k'^\mu}{2}\right)^{1/2} \quad (8)$$

is the energy of either photon in the center of momentum ([CM]) frame of the two photons, and u_{CM} is the four-velocity of the [CM] frame.

Equation 6 is invariant since $\sqrt{-g}d^3xdt$ is coordinate invariant, the distribution function is invariant (because d^3xd^3k is invariant), $\epsilon_{[\mathrm{CM}]}$ is a scalar, the cross section is invariant, and $d^3k/\sqrt{-g}k^t$ is invariant. It also reduces to the correct rate (cf. eq. 12.7 of Landau & Lifshitz, Classical Theory of Fields) in Minkowski space, and is therefore the correct general expression for the pair production rate. Because $\dot{n}_\pm$ itself is invariant it also describes the pair creation rate in the fluid frame.

We will also calculate the rate of four-momentum transfer from the radiation field to the plasma via pair creation:

$$G^\mu \equiv \frac{1}{\sqrt{-g}}\frac{dP^\mu_\pm}{d^3xdt} = A\frac{1}{2}\int \frac{d^3k}{\sqrt{-g}k^t}\frac{d^3k'}{\sqrt{-g}k'^t}\frac{dN_\gamma}{d^3xd^3k}\frac{dN_\gamma}{d^3xd^3k'}\,(k^\mu + k'^\mu)\,\epsilon^2_{[CM]}\sigma_{\gamma\gamma}c. \quad (9)$$

Here A is a constant that makes the equation dimensionally correct.

3.2. Monte Carlo estimate of pair creation rate

We evaluate the integrals (6) and (9) using a Monte Carlo estimate. Given a sample of photons on a time slice t within a small three-volume Δ^3x, a naive estimate is

$$\frac{1}{\sqrt{-g}}\frac{dN_\pm}{d^3xdt} \approx \frac{1}{2}\sum_{i\neq j}\left(\frac{w_i}{\Delta^3x}\right)\left(\frac{w_j}{\Delta^3x}\right)\frac{1}{\sqrt{-g}k^t_i}\frac{1}{\sqrt{-g}k^t_j}\epsilon^2_{[CM]}\sigma_{\gamma\gamma}c \quad (10)$$

where there are N_s superphotons in Δ^3x. The number of possible pairs of colliding superphotons scales is $O(N_s^2)$ and so does the computational cost. One might expect that the error would scale as $1/\sqrt{N_s^2}$ because there are $O(N_s^2)$ pairs, but this is wrong. There are only N_s independent samples and so the error scales as $1/\sqrt{N_s}$. We can obtain an estimate

with accuracy that is the same order as (10) at a cost that is $O(N_s)$ using

$$\frac{1}{\sqrt{-g}}\frac{dN_{\pm}}{d^3xdt} \approx \frac{1}{2}\frac{N_s-1}{2}\sum_{i\neq j}\left(\frac{w_i}{\Delta^3 x}\right)\left(\frac{w_j}{\Delta^3 x}\right)\frac{1}{\sqrt{-g}k_i^t}\frac{1}{\sqrt{-g}k_j^t}\epsilon^2_{[CM]}\sigma_{\gamma\gamma}c \tag{11}$$

An identical procedure can be used to evaluate G^{μ}.

3.3. Test problem

Does our Monte Carlo procedure accurately estimate the pair production rate? As a simple test, we consider two isotropic point sources of monoenergetic radiation in Minkowski space in Cartesian coordinates (so $\sqrt{-\mathrm{g}}=1$), and assume the optical depth to pair creation is small. Both sources emit photons of energy $4m_ec^2$.

We calculate the expected pair production rate (Equation 6) at each point and compare the result with the numerical solution provided by the radiative transfer code. The energy of two colliding photons in their center-of-momentum frame is a function of the cosine of the angle between the rays from the two sources: $\epsilon^2_{[CM]} = (1/2)(1-\mu)k^tk'^t$. The photon momentum space distribution are δ functions for monoenergetic point sources. The number density of photons at distance r from the source is $dN_\gamma/d^3x = \dot{N}_\gamma/(4\pi r^2 c)$, where each source produces photons at a rate $\dot{N}_\gamma$.

In Figure 2 we show a 2-D map of the Monte Carlo estimate of the pair production rate in the plane of the two sources. In Figure 3 we show a slice of the analytical and numerical pair production rates (upper panel) along the black contour line showed in Figure 2 together with the difference plot (lower panel). The error of the numerical solution declines as $N_s^{-1/2}$, as demonstrated in Figure 4, where N_s is the number of photon packets emitted by each source; the pair production code is working correctly.

4. RIAF scaling laws

What are the expected pair production rates? If we have a self-consistent model for a radiatively inefficient accretion flow and the implied radiation field, and we know M and $\dot{M}$, we can directly estimate the pair production rate. This may not be possible if a self-consistent model is unavailable—if, for example, the accretion rate is high and the models are radiatively efficient. An alternative is to use the *observed* spectrum and some assumptions about the source geometry to estimate the radiation field within the source, then use this to estimate the pair production rate. We will follow both lines of argument and show

that they are consistent for slowly accreting, weakly radiative models, then argue that the estimate based on the observed spectrum likely applies to more rapidly accreting models where radiative cooling is important.

$\dot{n}_\pm$ depends on the photon distribution over energy $E = \epsilon m_e c^2$ within the source. Our models produce a nearly power-law high energy spectrum of photons with high energy cutoff $\epsilon_{max} \gg 1$, so we set

$$\frac{dn}{dE} = \frac{n_0}{m_e c^2}\,\epsilon^\alpha e^{-\epsilon/\epsilon_{max}} \tag{12}$$

We evaluated the pair production rate numerically for this energy distribution, and fit to the result over $-3 < \alpha < 2$ and $10 < \epsilon_{max} < 160$, finding

$$\frac{\dot{n}_\pm}{n_0^2 \sigma_T c} \simeq \frac{1}{16} e^{2\alpha/3} (\frac{4}{3} + \epsilon_{max}^{\alpha/2})^4 \ln(\frac{\epsilon_{max}}{2}) \tag{13}$$

(see also Zdziarski 1985 for a similar expression in the $\epsilon_{max} \gg 1$ limit). At worst the fit is ≈ 2 too small for $\alpha \approx 0$ and $\epsilon_{max} = 160$. For $\alpha < -2$, which is typical of our models, the relative error is smaller than 60%.

For $\alpha > 0$ ($d \ln \nu L_\nu / d \ln \nu > 2$) most pair production occurs near ϵ_{max}, and $\dot{n}_\pm$ is sensitive to ϵ_{max}. For $\alpha < 0$, most pair production occurs near $m_e c^2$ in the center-of-momentum frame, there is an equal contribution from each logarithmic interval in energy, and the pair production rate is only logarithmically sensitive to ϵ_{max}.

Our models have $\alpha \lesssim -2$, so $\dot{n}_\pm$ is insensitive to ϵ_{max} and we can set $\dot{n}_\pm \sim n_0^2 \sigma_T c$, where n_0 is the effective number density of pair-producing photons $\sim L_{512}/(4\pi \mathcal{L}^2 m_e c^3)$, where $L_{512} \equiv \nu L_\nu(512\mathrm{keV})$. Then

$$\dot{n}_\pm \simeq \left(\frac{L_{512}}{m_e c^2} \frac{1}{\mathcal{L}^2 c}\right)^2 \sigma_T c \times f(\frac{r}{\mathcal{L}}, \mu). \tag{14}$$

where f is a dimensionless function and r and $\theta = \cos^{-1}\mu$ are the usual BL and KS radius and colatitude; recall that $\mathcal{L} = GM/c^2$ is a characteristic lengthscale.

What do we expect for the spatial distribution of pair production f? The pair-producing photons are made by upscattering synchrotron photons in a ring of hot gas near the innermost stable circular orbit (ISCO). Away from this ring the density of photons will fall off as $\sim 1/r^2$. In Equation 11, there is a geometrical factor ${\epsilon_{[\mathrm{CM}]}}^2/k_1^t k_2^t \propto 1 - \cos\psi$, where ψ is the angle between the photon trajectories in the coordinate frame. At large distance $\psi \lesssim 1$ so this factor is $\propto 1/r^2$, thus $\dot{n}_\pm \sim r^{-6}$. Because upscattered photons are beamed into the plane of the disk the pair production rate should fall off away from the midplane as the density, which can be fit with $\rho \sim \exp(-\theta/(2\sigma_\rho^2))$. So $\dot{n}_\pm \sim \exp(-\theta/(2\sigma_\pm^2))$, with $\sigma_\rho \sim \sigma_\pm$. In sum, we expect $f \sim \exp(-\theta/(2\sigma_\pm^2))/r^6$.

4.1. Scalings with model parameters

Now suppose we know the mass $M = m_8 M_8$ (where we define $M_8 \equiv 10^8 M_\odot$) and the accretion rate $\dot{M} = \dot{m}\dot{M}_{Edd}$, where $\dot{M}_{Edd} \equiv L_{Edd}/(\epsilon_{ref} c^2)$ and $\epsilon_{ref} = 0.1$ is a reference accretion efficiency. We will assume that photons are produced in a low frequency synchrotron peak and then scattered to $\sim 512\,\mathrm{keV}$ by n_{sc} Compton scatterings, where n_{sc} is 1 or 2.

For a plasma that is optically thin to synchrotron absorption at peak, the total number of synchrotron photons at the peak frequency produced per unit time is $\dot{N}_{\nu_{peak}} \simeq 4\pi\nu_{peak} j_{\nu_{peak}} \mathcal{L}^3/(h\nu_{peak})$, where $j_{\nu_{peak}}$ is the synchrotron emissivity [2]. The number density of synchrotron photons is then $n_{\nu_{peak}} \simeq \dot{N}_{\nu_{peak}}/(4\pi\mathcal{L}^2 c)$.

A fraction $\tau^{n_{sc}}$ of the peak photons are upscattered to 512 keV, where $\tau = \sigma_T n_e \mathcal{L}$ is the Thomson depth of the plasma, so $n_{512} = n_{\nu_{peak}} \tau^{n_{sc}}$. The mean number of Compton scatterings is $n_{sc} = \log(m_e c^2/h\nu_{peak})/\log A$, where $A \approx 16\Theta_e^2$ is the photon energy enhancement in single scattering by a relativistic electron, so

$$n_{sc} \simeq a_1 + a_2 \log \frac{m_8}{\dot{m}}. \tag{15}$$

We determine a_1 and a_2 numerically but for a reference model with $\dot{m} = 10^{-8}$ and $m_8 = 4.5 \times 10^{-2}$ (Sgr A*), the average value of $n_{sc} \approx 1 - 2$.

Assuming $\dot{M} \sim 4\pi\rho c\mathcal{L}$, the magnetic pressure is comparable to the gas pressure and both are $\sim \rho c^2$, the plasma density, magnetic field strength, and plasma temperature (close to the virial temperature) scale as

$$n_e \simeq \frac{1}{\epsilon_{ref}} \left(\frac{c^2}{GM_8\sigma_T}\right) \left(\frac{\dot{m}}{m_8}\right) \tag{16}$$

$$\frac{B^2}{8\pi} \simeq \frac{1}{\epsilon_{ref}} \left(\frac{m_p c^4}{GM_8\sigma_T}\right) \left(\frac{\dot{m}}{m_8}\right) \tag{17}$$

and

$$\Theta_e \simeq \frac{1}{30}\frac{m_p}{m_e}. \tag{18}$$

Combining, the pair production rate is

$$\dot{n}_\pm \simeq \mathcal{A} \left(\frac{1}{r_0^3 \mathcal{T}}\right) \epsilon_{ref}^{-(2n_{sc}+3)} \alpha_f^2 \frac{m_p}{m_e} \dot{m}^{3+2n_{sc}} f(\frac{r}{\mathcal{L}}, \mu), \tag{19}$$

where $\mathcal{A}$ is a constant to be determined numerically, $r_0 \equiv e^2/(m_e c^2)$ is the classical electron, α_f is the fine structure constant. From now on we will set $\epsilon_{ref}^{-(2n_{sc}+3)} = 10^{-6}$, i.e. $\epsilon_{ref} =$

[2] $j_{\nu_{peak}} \simeq 8\sqrt{2}e^3 n_e B/(27 m_e c^2)$, see Leung et al. 2010

0.1 and $n_{sc} = 3/2$; since n_{sc} depends logarithmically on $\dot{m}$ and m_8, this is equivalent to suppressing a weak power-law dependence on $\dot{m}$ and m_8. Then

$$\dot{n}_{\pm} \simeq 9 \times 10^{39}\ \mathcal{A}\ m_8^{-1}\ \dot{m}^6\ f(\frac{r}{\mathcal{L}}, \mu), \tag{20}$$

where we have assumed $n_{sc} = 3/2$.

For the estimating a jet kinetic luminosity it is useful to estimate the total rate at which pairs are produced:

$$\dot{N}_{\pm} = \int_{r>r_{hor}} \sqrt{-\mathrm{g}}\, d^3x\, \dot{n}_{\pm} \tag{21}$$

where r_{hor} is the horizon radius. Then

$$\dot{N}_{\pm} \simeq \dot{n}_{\pm}\mathcal{L}^3 \simeq 10^{78}\, \mathcal{A}\, \dot{m}^{3+2n_{sc}} m_8^2 \quad \mathrm{s}^{-1} \tag{22}$$

The number of pairs that escape to large radius ("free pairs") is a small multiple of this, and includes only those pairs that are made inside the funnel, at radius outside a stagnation radius r_{st}, inside which pairs fall immediately into the hole.

Evidently the pair production rate is very sensitive to the mass accretion rate, $\dot{n}_{\pm} \sim \dot{m}^6$. This steep dependence shuts off pair production at low accretion rates, and makes it difficult for $\dot{m}$ systems like Sgr A* to populate their funnel with pairs. Indeed, the pair production rate is so low that the implied charge density in the funnel likely falls below the Goldreich-Julian charge density (see §5.4).

4.2. Scalings with observables

Now suppose that we do not know the spectrum from first principles, but instead we know only M, the X-ray luminosity $L_X \equiv l_x L_\odot$ (assuming isotropic emission), and the X-ray spectral index $\alpha_X = d\log(\nu L_\nu)/d\log\nu|_{2-10keV}$.

If the spectrum is power-law from the X-ray up to MeV energy,

$$L_{512}(L_X) \approx L_X e^{4.92\alpha_X}, \tag{23}$$

$$\dot{n}_{\pm} \approx \mathcal{B}\ \left(\frac{c^3\sigma_T L_\odot^2}{m_e^2 G^4 M_8^4}\right)\ l_X^2\ e^{(9.26\alpha_X)}\ m_8^{-4}\ f(\frac{r}{\mathcal{L}}, \mu) \tag{24}$$

where $\mathcal{B}$ is a constant to be determined numerically and $(c^3\sigma_T L_\odot^2/m_e^2 G^4 M_8^4) \approx 10^{-8}\ \mathrm{cm}^{-3}\mathrm{s}^{-1}$.

The total rate at which pairs are produced is

$$\dot{N}_{\pm} \simeq \dot{n}_{\pm}\mathcal{L}^3 \simeq \mathcal{B}\ (\frac{\sigma_T L_\odot^2}{m_e^2 G M_8 c^3})\ l_X^2\ e^{9.26\alpha_X}\ m_8^{-1} \tag{25}$$

where $(\sigma_T L_\odot^2/m_e^2 G M_8 c^3) = 10^{31}$ s^{-1}. The dependence on black hole mass changes between Equations (24) and (25) because $\mathcal{L} \propto m_8$.

5. Pair production in RIAF - numerical results

We are now in a position to evaluate the pair production rate numerically, check whether it matches the expected scaling laws, and evaluate $f(r,\mu)$. To do this, we have run simulations with a range of M and $\dot{M}$, assuming that the models have equal ion and electron temperatures, $T_e = T_i$. A list of model parameters is given in Table 1.

5.1. Pair creation rate

5.1.1. Dependence on model parameters: $\dot{m}$, m

The spatial distribution of $\dot{n}_\pm$ in models A through H (see Table 1) is well fit by

$$\dot{n}_\pm(r,\mu) = 3\times 10^{40}\dot{m}^{3+2n_{sc}} m_8^{-1} \times (\frac{r}{\mathcal{L}})^{-6} e^{-\mu^2/(2\sigma_\pm^2)}\,\mathrm{cm}^{-3}\,\mathrm{s}^{-1} \tag{26}$$

that is $\mathcal{A} \simeq 3$ in equation (20), where again we set $\epsilon_{ref}^{-3-2n_{sc}} = 10^{-6}$. The constant in Equation 26 is estimated assuming that the electrons and ions are well coupled and $T_\mathrm{i}/T_\mathrm{e} = 1$. It is worth noting that the constant drops sharply for higher temperature ratios; e.g. for $T_\mathrm{i}/T_\mathrm{e} = 3$, it is 10^{-4} times smaller.

The dependence $\dot{n}_\pm \sim r^{-6}$ at large radius, as expected. Surprisingly, this power law provides a good fit to the pair production rate all the way in to the horizon. It follows that the abundance of free pairs will depend sensitively on the structure of the magnetosphere at the stagnation radius r_{st}.

The pair production scale height $\sigma_\pm \approx 0.3$ independently of $\dot{m}$, m. This is nearly identical to σ_ρ, the plasma scale height. Notice that $\sigma_\pm$ also controls the fraction produced inside the funnel f_{jet}; typically f_{jet}=10%. The funnel wall is at

$$\mu^2 = \mu_f^2 = \frac{r + 0.4GM/c^2}{r + 4GM/c^2}. \tag{27}$$

Figure 5 shows a 2D contour map of $\dot{n}_\pm$ corresponding to model C and the analytic fit to the time averaged distribution of $\dot{n}_\pm$, along with a contour marking the approximate boundary of the funnel. The grid averaged fractional difference between time averaged MHD models

A through H and analytical formula given by Equation (26) is $< 60\%$. Since $\dot{n}_{\pm}$ is a steeply declining function of μ^2, almost all free pairs are made near the funnel walls.

A fit to the total number of pairs produced (not the total number of free pairs; this include pairs produced in the accretion flow near the equatorial plane) yields

$$\dot{N}_{\pm} = 4 \times 10^{80} \dot{m}^{3+2n_{sc}} m_8^2 \, \mathrm{s}^{-1} \tag{28}$$

where $n_{sc} = 1. + 0.03 \log m_8/\dot{m}$. Figure 6 presents the comparison of the time averaged numerical estimate of $\dot{N}_{\pm}$ from MHD runs to the fitting formula given by Equation 28, without the factor f_{jet}.

5.1.2. Dependence on observable parameters: l_X, α_X, m

Our numerical experiments show that $\dot{n}_{\pm}$ depends on l_X, α_X, and m according to

$$\dot{n}_{\pm}(r,\mu) = 10^{-8} \, l_X^2 e^{9.26\alpha_X} m_8^{-4} \times (\frac{r}{\mathcal{L}})^{-6} e^{-\mu^2/2\sigma_{\pm}^2} \ \mathrm{cm}^{-3} \, \mathrm{s}^{-1}. \tag{29}$$

i.e. $\mathcal{B} \simeq 1$ in Equation (24). The fractional difference between the numerical results and above formula is $< 50\%$ for time averaged models A-L. The total number of pairs created in the system is

$$\dot{N}_{\pm} = 5 \times 10^{30} \, l_X^2 e^{(9.26\alpha_X)} m_8^{-1} \ \mathrm{s}^{-1} \tag{30}$$

Figure 7 compares $\dot{N}_{\pm}$ to the semianalytic formula given by Equation 30 for different snapshots of the simulations with different mass accretion rates (models A-C) and black hole masses (models F-H). The semianalytic and numerical results agree well, and the scaling constants are close to those estimated in §4.

5.2. Pair power and electromagnetic luminosity of a funnel

We define the "luminosity" of pair creation in the funnel as

$$L_{\pm} = f_{jet} \dot{N}_{\pm} 2 m_e c^2 \Gamma_{jet} \tag{31}$$

where f_{jet} is a fraction of pairs produced in the magnetically dominated funnel, and Γ_{jet} is the jet bulk Lorentz factor at large radius (this assumes cold flow). As a function of model parameters,

$$L_{\pm} \simeq 6 \times 10^{74} f_{jet} \dot{m}^{3+2n_{sc}} m_8^2 \Gamma_{jet} \, \mathrm{ergs} \, \mathrm{s}^{-1} \tag{32}$$

and in terms of the X-ray luminosity and X-ray spectral index

$$L_{\pm} \simeq 10^{25} f_{jet} l_X^2 e^{9.26\alpha_X} m_8^{-1} \Gamma_{jet} \,\mathrm{ergs\,s^{-1}} \tag{33}$$

It is interesting to compare this with the Blandford-Znajek (BZ), or electromagnetic, luminosity of the funnel

$$L_{BZ} = 2\pi \int_{\sigma_{mag}>1} d\theta \sqrt{-g} T_t^r \tag{34}$$

where $T_t^r = b^2 u^r u_t - b^r b_t$ is the electromagnetic part of the stress-energy tensor and is computed directly from the numerical simulation data. We integrate the flux through the horizon only in the magnetically dominated region ($\sigma_{mag} > 1$; the peak magnetic flux per unit "area" is on the equator, and declines toward the pole, so the peak flux in the funnel is along the funnel wall).

The BZ luminosity is calculated numerically using formula 34 and we find the following fitting function expressed in terms of the model parameters:

$$L_{BZ} \approx 8 \times 10^{45} (1 - \sqrt{1 - a_*^2})^2 \,\dot{m}\, m_8 \;\; \mathrm{ergs\,s^{-1}} \tag{35}$$

The electromagnetic luminosity scale factor $\sim \mathcal{ML}^2/\mathcal{T}^3$, and we need to introduce additional m_8 in the scaling formula, because $\dot{M}_{Edd} \sim M$. The scaling with the a_* is taken from Equation (61) of McKinney & Gammie 2004, which is a fit to their numerical data.

Then for Sgr A* mass and $a_* = 0.94$, $L_{BZ} > L_{\pm}/\Gamma_{jet}$ for $\dot{m} < \dot{m}_{crit} \approx 10^{-6}$ (for $\dot{m}_{crit}$ see § 6.1). At low accretion rates the BZ luminosity completely dominates the pair luminosity, because the pair luminosity is such a steep function of accretion rate. Notice that, because $L_{\pm} \sim m_8^2$ while $L_{BZ} \sim m_8$, the $\dot{m}$ at which two luminosities are equal, is higher for lower mass black holes. $L_{\pm}/L_{BZ}$ ratio is shown in the Table 1. We conclude that, unless $\Gamma_{jet} \gg 1$, the funnel luminosity is electromagnetically dominated for most radiatively inefficient flows.

5.3. Energy-momentum deposition

Some of the pairs created in the funnel will escape to large radius and some will fall into the black hole. In an MHD model, the escaping fraction and asymptotic Lorentz factor will depend on the run of pair creation rate with radius, the magnetic field structure, the energy density of the pair plasma, and the pair-creation four-force G^{μ}.

Based on numerical calculations the spatial distribution of G^{μ} is well fit, with $x \equiv r/\mathcal{L}$, by

$$G^0_{code}(r,\mu) = G^0 \frac{\mathcal{L}^2\mathcal{T}^2}{\mathcal{M}} \approx \frac{300}{x} \, \frac{\dot{n}_{\pm}(x,\mu) m_e c}{\mathcal{M}/(\mathcal{L}^2\mathcal{T}^2)} \tag{36}$$

$$G^1_{code}(x,\mu) = G^1 \frac{\mathcal{L}^2\mathcal{T}^2}{\mathcal{M}} \approx \frac{20(x-x_{st})}{x^2}\ \frac{\dot{n}_\pm(x,\mu)m_e c}{\mathcal{M}/(\mathcal{L}^2\mathcal{T}^2)} \tag{37}$$

$$G^2_{code}(x,\mu) = G^2 \frac{\mathcal{L}^2\mathcal{T}^2}{\mathcal{M}} \approx \frac{\mu}{x^2}\ \frac{\dot{n}_\pm(x,\mu)m_e c}{\mathcal{M}/(\mathcal{L}^2\mathcal{T}^2)} \tag{38}$$

$$G^3_{code}(x,\mu) = G^3 \frac{\mathcal{L}^2\mathcal{T}^2}{\mathcal{M}} \approx \frac{150}{x^2}\ \frac{\dot{n}_\pm(x,\mu)m_e c}{\mathcal{M}/(\mathcal{L}^2\mathcal{T}^2)} \tag{39}$$

where $\mathcal{M}, \mathcal{T}, \mathcal{L}$, and $\dot{n}_\pm$ are given in cgs units. The four-force vector components are given in a Kerr-Schild coordinate basis and in code units; we divide G^μ in cgs units by the unit of the four-force density $\mathcal{M}/\mathcal{L}^2\mathcal{T}^2$. All components of the four-force depend more steeply on radius than $\dot{n}_\pm$. The radial component of the four-force is positive at large radius, zero at $x_{st} \approx x_{ISCO}(1+\mu^2/2)$, and negative at small radius. The sign of G^2 changes at the equatorial plane, as it should.

Pairs are created in the funnel with an initial distribution function. This distribution is immediately isotropized with respect to rotation around the magnetic field line. Later evolution of the distribution function will depend on ill-understood relaxation processes; the pairs may not relax. Whether or not relaxation occurs the initial mean energy of the particles is of interest. So: what is the energy distribution of the created pairs $d\dot{n}_\pm/d\log\gamma_{e^\pm[FF]}$, where $\gamma_{e^\pm[FF]}$ is the Lorentz factor of new particles measured in the fluid frame [FF]?

Four-momentum is conserved in the pair-creation process, so the average Lorentz factor of the new leptons in the fluid frame is

$$\gamma_{e^\pm[FF]} = -\frac{1}{2} u_\mu (k^\mu + k'^\mu) \tag{40}$$

where u_μ is four-velocity of the background plasma and we assume that k^μ is in units of $m_e c^2$. Figure 8 shows $d\dot{n}_\pm/d\log\gamma_{e^\pm[FF]}$ in model C at three different radii $r = r_h, r_{isco}, 5R_g$ (averaged over 20 radial zones from $\theta = 0-10$ deg for higher signal-to-noise; here $r_h \equiv$ event horizon radius). The injected energy distribution peaks at $\gamma_{e^\pm[FF]} \sim$ a few and has a cut-off at $\gamma_{e^\pm[FF]max} \approx 100$.

If the thermalization timescale is short (which, given the low density and likely high temperature of the plasma, seems unlikely to us), then the rate of internal energy injection due to $e^\pm$ creation is $\dot{u} = \dot{e}_\pm$, where the kinetic energy density injection rate, in the plasma frame, is [3]

$$\dot{e}^\pm = \int d\gamma_{e^\pm[FF]}\,(\gamma_{e^\pm[FF]} - 1)\, m_e c^2\, \frac{d\dot{n}_\pm}{d\gamma_{e^\pm[FF]}} \tag{41}$$

[3]The same $\dot{e}_\pm$ can be obtained by transforming G^μ from coordinate into the fluid frame and subtracting the rest mass energy.

The corresponding temperature of the newly injected pairs is $\Theta_{e^\pm} = (1/3)\dot{e}_\pm/(\dot{n}_\pm m_e c^2) \approx 20, 10, 3$ at $r = r_h, r_{isco}$, and $5M$, respectively. This temperature is slightly below that of the thermal background plasma, and is sub-virial. Pairs are not born hot.

The entropy of the injected pairs is likely to increase over the initial entropy. The funnel is exposed to "acoustic" radiation from the accretion disk. A small fraction of the MHD waves generated by turbulence in the disk will propagate toward the funnel, be transmitted at the funnel wall, and dissipate within the funnel. Because the density of the funnel is so low, even a small fraction of the disk acoustic luminosity is capable of raising the pair plasma temperature to $\Theta_e \gg 1$ before it can escape at Lorentz factor $\Gamma^2_{jet} \gg 1$. Until the magnitude of turbulent heating can be estimated, the dynamics of the funnel pair plasma is extremely uncertain.

5.4. Comparison to Goldreich-Julian density

Is the charge number density implied by $\dot{n}_\pm$ sufficient to enforce the ideal MHD condition $\mathbf{E} = \mathbf{0}$ in the rest frame of the plasma ($u_\mu F^{\mu\nu} = 0$): does the pair number density exceed the Goldreich-Julian density n_{GJ}?

A naive estimate of n_{GJ} uses the flat-space Goldreich-Julian charge number density

$$n_{GJ} \simeq \frac{\Omega B}{4\pi e c} = \frac{a_* B c^2}{32\pi G M e} \tag{42}$$

where the field rotation frequency in the funnel $\Omega = (a_*/8)c^3/(GM)$ in the Blandford-Znajek model at $a_* \lesssim 1$. For our standard Sgr A* model with $B \sim 30$G, $a_* \simeq 0.94$, $M \simeq 4.5\times10^6 \mathrm{M}_\odot$, this yields $n_{GJ} \simeq 10^{-3}\,\mathrm{cm}^{-3}$.

A better estimate uses the Blandford-Znajek model for a monopole magnetosphere. We use Kerr-Schild coordinates (t, r, θ, ϕ) and define the Goldreich-Julian density as the charge density measured in the frame of the normal observer, who to lowest (zeroth) order in a_* has four-velocity $n_\mu = (-(1 + 2/r)^{-1/2}, 0, 0, 0)$. Using the current density J^μ derived from the BZ monopole solution as given in McKinney & Gammie (2004) we find, to lowest order in a_*,

$$n'_{GJ} \equiv -n_\mu J^\mu = \frac{a_* B^r c^2}{4\pi G M e}\,\frac{(1 + 2/x)^{1/2}\cos\theta}{x^3} \tag{43}$$

where again $x \equiv r/\mathcal{L}$ and B^r is the radial component of the field at $x = 1$ (see McKinney & Gammie 2004 for a definition of B^r). This is very close to the naive estimate. Notice that $n'_{GJ} \sim B^r \cos\theta$ so the charge density changes sign from one hemisphere to the other. This is an artifact of the monopole model. If instead the field is allowed to change sign from one

hemisphere to the other, but within each funnel is modeled as a monopole then the sign is consistent. Also notice that $n'_{GJ} \sim 1/r^3$, so the requirement on charge density is strongest close to the horizon even if the magnetosphere contains a wind with $n \sim 1/r^2$.

A still better estimate for n_{GJ} would use the simulation-derived currents. We have calculated these and the charge densities are consistent with the estimates just given. Using estimates for B^r from § 4, we can derive a scaling with $\dot{m}$ and m:

$$n_{GJ} \sim 3 \times 10^{-1}\, a_*\, \dot{m}^{1/2} m_8^{-3/2} \ \ \mathrm{cm}^{-3} \tag{44}$$

near $x = 2$, and a ratio of this to a characteristic number density of pairs near the horizon at the funnel axis $n_\pm \sim \dot{n}_\pm \mathcal{T} \approx 5 \times 10^{40} \dot{m}^6$ (using Equation 26 and $\mu = 1$):

$$\frac{n_{GJ}}{n_\pm} \sim 6 \times 10^{-42}\, a_* \dot{m}^{-11/2} m_8^{-3/2}. \tag{45}$$

Again this is the ratio on the axis. Although the Goldreich-Julian density varies only weakly across the funnel, the pair production rate in our fiducial model is about 20 time larger at the funnel wall at $x \sim 2$. At very low $\dot{m}$, where $n_{GJ} \sim n_\pm$, the center of the funnel is populated by some other process—perhaps a pair cascade— and the edges by pair production in $\gamma\gamma$ collisions.

6. Discussion

6.1. Selfconsistency of the models

Our models are selfconsistent with they are both radiatively inefficient and the implied pair density $\dot{n}_\pm \mathcal{T}$ is greater than the Goldreich-Julian density. Figure 9 shows the parameter range for which our scalings for production of $e^\pm$ pairs in the funnel are fully selfconsistent (shaded region). The solid line represents models for which pairs density equals the n_{GJ} density near the horizon for black hole spin $a_* = 0.94$, assuming that pairs escape from the funnel on the light crossing time. The model is radiatively inefficient when $L_{Bol}/\dot{M}c^2 \lesssim 0.1$. The efficiency of $\simeq 10\%$, can be translated into a critical value of $\dot{m}$. Our numerical estimates give $\dot{m}_{crit} \approx 10^{-6}$ if $T_\mathrm{i}/T_\mathrm{e} = 1$. In Figure 9, the $\dot{m}_{crit}$ is marked as a vertical dashed line (for $T_\mathrm{i}/T_\mathrm{e} > 1$, $\dot{m}_{crit}$ increases). Our models are therefore fully selfconsistent in a wedge in parameter space, and are never applicable to stellar mass black holes. The estimates for pair production rates based on the observed X-ray luminosity may nevertheless be applicable even in radiatively efficient accretion flows.

6.2. Sgr A*

A bright radio source associated with a supermassive black hole ($M_{BH} = 4.5 \times 10^6 \mathrm{M}_\odot$) in the Galactic center, Sgr A*, is a weak X-ray source ('quiescent' emission $L_X \lesssim 10^{33} \mathrm{ergs\,s^{-1}}$) and it is strongly sub-Eddington ($L/L_{Edd} \approx 10^{-9}$). To model Sgr A*, we refer to Mościbrodzka et al. (2009), which suggests the most probable spin of the black hole $a_* = 0.94$, temperature ratio $T_i/T_e = 3$, and $\dot{m} = 2 \times 10^{-8}$. The $\dot{n}_\pm$ rate for these parameters is slightly lower than in the scaling laws because of $T_\mathrm{i}/T_\mathrm{e} \neq 1$. For the purposes of this subsection only, we consider 3D models which, it turns out, have $\dot{n}_\pm$ very similar to the 2D models. All models assume the accretion flows lies in the equatorial plane of the black hole. The emergent radiation is calculated using the Monte Carlo code `grmonty` (Dolence et al. 2009).

During the quiescent state the X-ray luminosity is $l_X < 1$ and pair production near the horizon in the funnel, in model I, is $\dot{n}_\pm \approx 10^{-9}\,\mathrm{s^{-1}}$, measured directly from the simulations. The corresponding light crossing time is $\mathcal{T} \approx 20$s, and so a typical pair density near the horizon in the funnel is $n_\pm \approx 10^{-8}\mathrm{cm^{-3}}$. This is five orders of magnitude below $n_{GJ} \approx 10^{-3}\mathrm{cm^{-3}}$. In quiescence the funnel must therefore be populated by a process other than $\gamma\gamma$ pair production process considered here, for example a pair cascade.

It is known, however, that Sgr A*exhibits intraday variability at all observed wavelengths (radio, sub-mm, NIR, and X-rays). In particular in the X-ray band (2-10 keV) luminosity may increase up to 160 times (e.g. the brightest flare detected has luminosity of $L_X = 5.4 \times 10^{34}$ Porquet et al. 2008) from the 'quiescent' level and last a few ks. During such a bright flare the X-ray slope can change, and the pair production rate may reach or exceed n_{GJ}. Even during a flare the funnel kinetic luminosity is far below the Blandford-Znajek luminosity (see Table 1) for any reasonable Γ_{jet}. We conclude that close to the black hole any jet in Sgr A* is electromagnetically dominated.

6.3. M87

The core of M87 hosts a sub-Eddington supermassive black hole, $M_{BH} = 3 \times 10^9 \mathrm{M}_\odot$ (Marconi et al. 1997, but see Gebhardt & Thomas 2009). M87 has a prominent radio jet resolved from $100GM/c^2 - 1$kpc. Models in which the jet is a pair plasma appear to be more consistent with the data than models in which the jet is composed of ion-electron plasma (Reynolds et al. 1996). The application of our models to this object is difficult because the SED of M87 emitted from the inner 100 R_g is most likely contaminated by the emission from the jet.

As in Sgr A*, for M87 we assume a_*=0.94. The inclination of disk with respect to the

observer, $i = 30\,\mathrm{deg}$ (Heinz & Begelman 1997), and again we assume that the accretion disk lies in the equatorial plane of the black hole, that the electron distribution function is thermal, and that $T_\mathrm{i}/T_\mathrm{e} = 3$. The modeled SED of M87 is normalized via $f_\nu(\nu = 230\,\mathrm{GHz}) = 2\mathrm{Jy}$ at 17 Mpc (Tan et al. 2008). We find that the zero cooling, 2D model with $\dot{m} = 1.5 \times 10^{-6}$ (model K) which can reproduce the 230 GHz flux, have too large a radiative efficiency to be consistent with RIAF assumptions (see Table 1).

To model the source selfconsistently, we have run axisymmetric models that include synchrotron cooling in the dynamical evolution of the accretion disk (model L). This procedure reduces the radiative efficiency by a factor of 100, to $\sim 30\%$, which is still too high, but much closer to self-consistency. Future models will incorporate both synchrotron cooling and Compton cooling. For model L, $L_X = 10^{41}\mathrm{ergss}^{-1}, L_\pm = 7 \times 10^{36}\mathrm{ergss}^{-1}$, and $L_{BZ} \approx 10^{41}\mathrm{ergss}^{-1}$.

We find that the spatial distribution of pair production is very similar to that in models without cooling. In model L, the implied pair density $n_\pm = \dot{n}_\pm \mathcal{T} \approx 10\,\mathrm{cm}^{-3}$ ($\mathcal{T} \approx 10^4$ s), which is 10^7 times larger than $n_{GJ} \approx 10^{-6}\mathrm{cm}^{-3}$ in almost the entire computational domain. The pair luminosity in both models K and L is still smaller than electromagnetic luminosity by factor of 0.1 and 10^{-5}, respectively. The base of the jet is optically thin, $\tau_\pm \approx n_\pm \mathcal{L} \sigma_T \approx 10^{-10}$ for pair annihilation.

A separate, more nearly model-independent, estimate of the total pair production rate can be obtained from the X-ray spectrum of M87 using Equation (30). We use $L_X \simeq 3 \times 10^{41}$; this is the 7×10^{40} from Di Matteo et al. (2003) corrected upward to an isotropic X-ray luminosity because our models emit X-rays anisotropically into the equatorial plane. We also set $\alpha_X = 0$. Then $\dot{N}_\pm \simeq 10^{45}\mathrm{s}^{-1}$, which implies $L_K = f_{jet} \dot{N}_\pm m_e c^2 \Gamma_{jet} = 8 \times 10^{38} \Gamma_{jet} f_{jet}$. This is too small to account for the estimated kinetic luminosity of the jet for $f_{jet} < 0.1$ (and probably closer to 0.01; the fraction of free pairs depends on the dynamics of pairs close to the horizon) and $\Gamma_{jet} < 100$, since L_K is estimated to be $> 3 \times 10^{42}\mathrm{ergss}^{-1}$ (Young et al. 2002). Notice that our nearly consistent model L has $L_{BZ} \simeq 10^{41}\mathrm{ergss}^{-1}$.

Can the M87 jet be composed of pairs? The alternatives are (1) the jet is composed of pairs and they are not produced by $\gamma\gamma$ collisions close to the black hole. For example, there could be direct particle acceleration to large Γ that permits pair production from low energy photons. (2) the jet is composed of pairs but the black hole in M87 has $a_* > 0.93$, and increasing spin sharply increases the pair production rate, both for models that infer $\dot{N}_\pm$ from a fully self-consistent model, and those that infer $\dot{N}_\pm$ from X-ray measurements. This is consistent with our preliminary investigations of dependence of pair production rate on spin; (3) the jet is composed of pairs but our models simply miss or mis-estimate an important physical feature of the flow. This scenario has to contend with the direct estimate

of the pair production rate from M87's spectrum in the last paragraph, which suggests that the pair production rate is too low by > 1.5 orders of magnitude; (4) the jet is composed of pairs, but the observational estimates of the jet kinetic luminosity are too large; (5) the jet is composed of an electron-ion plasma, which may be accelerated in the funnel walls.

7. Summary

We have studied the electron-positron pair production rates in the black hole magnetospheres by $\gamma\gamma$ collisions. Our pair productuon rates simulations are based on a GRMHD time dependent model of magnetized disk around spinning black hole. The disk is a source of high energy radiation formed in multple Compton scatterings of synchrotron photons. We performed nearly *ab-initio* calculations of the photon-photon collisions rates within $40GM/c^2$ of the event horizon, using Monte Carlo techniques.

Our main result are the analytical formulas for spatial distribution of pair production rates, which normalizing factor is a well defined function of the global parameters of the system (m,$\dot{m}$,L_X,α_X). The pair plasma is injected with a power-law- like energy distribution. Most of pair plasma is created in the equatorial plane of the thick disk, due to strong Doppler beaming of radiation. The pair plasma has neqligible effect on the RIAF dynamical evolution which is consistent with previous results by Esin 1999 and Kusunose & Mineshige 1996, if the pair plasma density in the disk is estimated assuming that it escapes on viscous time scale instead of in light crossing time scale (i.e. it is coupled to the disk plasma).

Only a few percent of all pairs are created in the magnetized funnel (black hole magnetosphere), and most of pairs in the funnel are created near its wall. Pair jets are optically thin for photons with frequencies $\nu > \nu_t = 10^{-3} n_{\pm} \mathcal{L}$ Hz (for example, for M87 $\mathcal{L} = 4 \times 10^{14}$, and $n_{\pm} = 10$, turnover frequency $\nu_t = 10^{12}$ Hz).

We also find than the general relativistic RIAF models are selfconsistent up to $\dot{m}_{crit} \approx 10^{-6}$, which is a little smaller than e.g. $\dot{m}_{crit} = 5 \times 10^{-6}$ reported by Fragile & Meier 2009. For higher $\dot{m}$ one must couple the radiation evolution into the dynamical model.

Models with $\dot{m} < \dot{m}_{crit}$ have force-free, Thomson thin jets with the Blandford-Znajek luminosity much larger than pair kinetic luminosity. In models with very small $\dot{m}$, the pair plasma density in the funnel is much lower than the Goldreich-Julian density, suggesting that another process, such as a pair cascade, will operate and populate the funnel.

We have avoided discussing spin dependence to limit the size of the parameter space, but our preliminary investigations suggest that $\dot{n}_{\pm}$ is very sensitive to spin. Higher spin

black holes are smaller and therefore have higher compactness, and at fixed accretion rate tend to have harder spectra.

REFERENCES

Beckwith, K., Hawley, J. F., & Krolik, J. H. 2008, ApJ, 678, 1180

Beskin, V. S., Istomin, Y. N., & Par'ev, V. I. 1992, AZh, 69, 1258

Blandford, R. D. & Znajek, R. L. 1977, MNRAS, 179, 433

De Villiers, J., Hawley, J. F., & Krolik, J. H. 2003, ApJ, 599, 1238

Di Matteo, T., Allen, S. W., Fabian, A. C., Wilson, A. S., & Young, A. J. 2003, ApJ, 582, 133

Dolence, J. C., Gammie, C. F., Mościbrodzka, M., & Leung, P. K. 2009, ApJS, 184, 387

Dolence, J. C., Gammie, C. F., & Shiokawa, H. 2010, ApJ, 1, 1

Esin, A. A. 1999, ApJ, 517, 381

Fishbone, L. G. & Moncrief, V. 1976, ApJ, 207, 962

Fragile, P. C. & Meier, D. L. 2009, ApJ, 693, 771

Gammie, C. F., McKinney, J. C., & Tóth, G. 2003, ApJ, 589, 444

Gebhardt, K. & Thomas, J. 2009, ApJ, 700, 1690

Goldreich, P. & Julian, W. H. 1969, ApJ, 157, 869

Hawley, J. F. & Krolik, J. H. 2006, ApJ, 641, 103

Heinz, S. & Begelman, M. C. 1997, ApJ, 490, 653

Hirotani, K. & Okamoto, I. 1998, ApJ, 497, 563

Johnson, B. M. & Quataert, E. 2007, ApJ, 660, 1273

Komissarov, S. S. 2005, MNRAS, 359, 801

Krolik, J. H. 1999, Active galactic nuclei : from the central black hole to the galactic environment, ed. Krolik, J. H.

Kusunose, M. & Mineshige, S. 1996, ApJ, 468, 330

Leung, P., Gammie, C. F., & Noble, S. 2010, ApJ, 1, 1

Marconi, A., Axon, D. J., Macchetto, F. D., Capetti, A., Sparks, W. B., & Crane, P. 1997, MNRAS, 289, L21

McKinney, J. C. & Gammie, C. F. 2004, ApJ, 611, 977

Mościbrodzka, M., Gammie, C. F., Dolence, J. C., Shiokawa, H., & Leung, P. K. 2009, ApJ, 706, 497

Narayan, R. & Yi, I. 1994, ApJ, 428, L13

Phinney, E. S. 1983, PhD thesis, , Univ. Cambridge, (1983)

Phinney, E. S. 1995, in Bulletin of the American Astronomical Society, Vol. 27, Bulletin of the American Astronomical Society, 1450

Porquet, D., Grosso, N., Predehl, P., Hasinger, G., Yusef-Zadeh, F., Aschenbach, B., Trap, G., Melia, F., Warwick, R. S., Goldwurm, A., Bélanger, G., Tanaka, Y., Genzel, R., Dodds-Eden, K., Sakano, M., & Ferrando, P. 2008, A&A, 488, 549

Reynolds, C. S., Fabian, A. C., Celotti, A., & Rees, M. J. 1996, MNRAS, 283, 873

Sharma, P., Hammett, G. W., Quataert, E., & Stone, J. M. 2006, ApJ, 637, 952

Stepney, S. & Guilbert, P. W. 1983, MNRAS, 204, 1269

Tan, J. C., Beuther, H., Walter, F., & Blackman, E. G. 2008, ApJ, 689, 775

Vincent, S. & Lebohec, S. 2010, MNRAS, 1256

Young, A. J., Wilson, A. S., & Mundell, C. G. 2002, ApJ, 579, 560

Table 1. List of GRMHD models.

ID	a_*	m_8	$< \dot{m} >_t$	L_{Bol}/L_{Edd}	radiative efficiency	$L_{\pm}/(L_{BZ}\Gamma_j)$	note
A	0.94	4.5×10^{-2}	2×10^{-9}	10^{-11}	7×10^{-4}	10^{-17}	2D
B	0.94	4.5×10^{-2}	6×10^{-9}	10^{-10}	2×10^{-3}	10^{-15}	2D
C	0.94	4.5×10^{-2}	1×10^{-8}	4×10^{-10}	4×10^{-3}	10^{-13}	2D
D	0.94	4.5×10^{-2}	5×10^{-8}	2×10^{-8}	0.02	10^{-10}	2D
E	0.94	4.5×10^{-2}	1×10^{-7}	6×10^{-8}	0.04	10^{-8}	2D
F	0.94	4.5×10^{-3}	1×10^{-8}	5×10^{-10}	5×10^{-3}	10^{-14}	2D
G	0.94	4.5×10^{-1}	1×10^{-8}	4×10^{-10}	4×10^{-3}	10^{-12}	2D
H	0.94	4.5	1×10^{-8}	3×10^{-8}	3×10^{-3}	10^{-11}	2D
				Sgr A*			
I	0.94	4.5×10^{-2}	2.7×10^{-8}	5×10^{-10}	2×10^{-3}	10^{-11}	3D-quiescent,$T_{\rm i}/T_{\rm e} = 3$
J	0.94	4.5×10^{-2}	5.3×10^{-8}	1×10^{-9}	3×10^{-3}	10^{-9}	3D-weak flare, $T_{\rm i}/T_{\rm e} = 3$
				M87			
K	0.94	30	1.5×10^{-6}	3×10^{-4}	16.5	0.1	2D - w/o cooling
L	0.94	30	1×10^{-6}	3×10^{-6}	0.3	4×10^{-5}	2D - w/ syn cooling

Note. — From left to right columns are: model ID, dimensionless spin of the black hole, the black hole mass in units of $M_\odot$, the rest mass accretion rate through the black hole horizon in units of Eddington mass accretion rate ($\dot{M}_{Edd} = 2.22 m_8$ M$_\odot$yr^{-1}) averaged over later times of the simulation ($\Delta t = 1500 - 2000\mathcal{T}$), the Eddington ratio L_{Bol}/L_{Edd}, the model radiative efficiency $\eta = L_{Bol}/\dot{M}c^2$ (L_{Bol} is the RIAF luminosity integrated over emitting angles and frequencies), ratio of Kinetic to electromagnetic luminosity, and comments on models. Models I & J correspond to Sgr A*while K&L model core of M87. Run L accounts for synchrotron cooling terms in the dynamical solution so the pair production rate is slightly reduced.

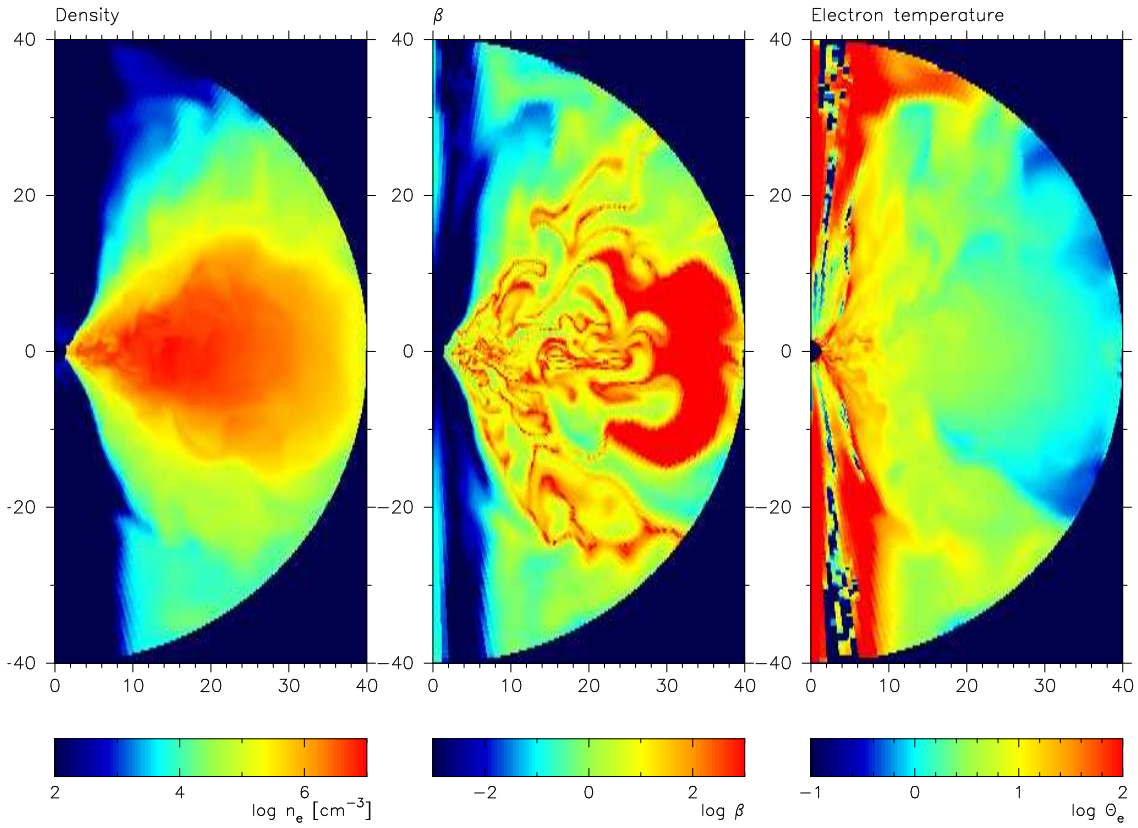

Fig. 1.— Structure of RIAF. Panels from left to right: density distribution, β plasma parameter, and dimentionless temperature, respectively.

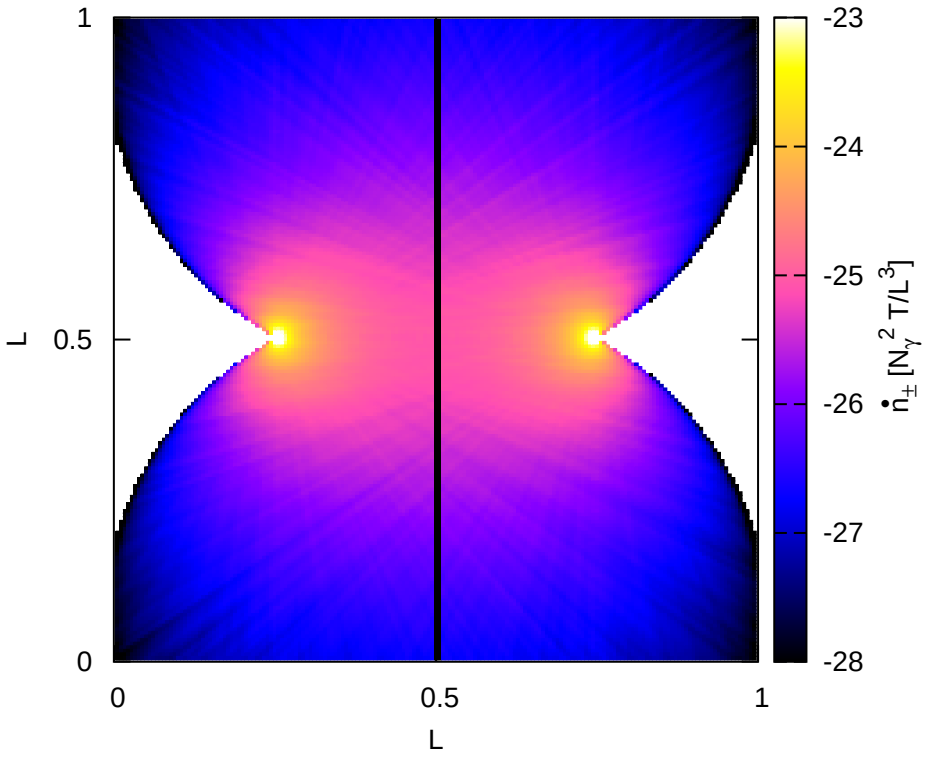

Fig. 2.— Test problem: the pair production rate in a plane of two, isotropic point sources of high energy radiation ($k_1^t = k_2^t = 4m_e c^2$). Pair production rate is given here in units of $\dot{N}_\gamma^2 T/L^3$, where L is a length unit, $\dot{N}_\gamma$ is a number of photons produced by each source per unit time T. Pair production rate is zero in two side regions because the energy of photons in the center-of-momentum frame is below the threshold energy there. The pair production rate is symmetric with respect to the axis connecting two sources. Black contour - see Fig 3.

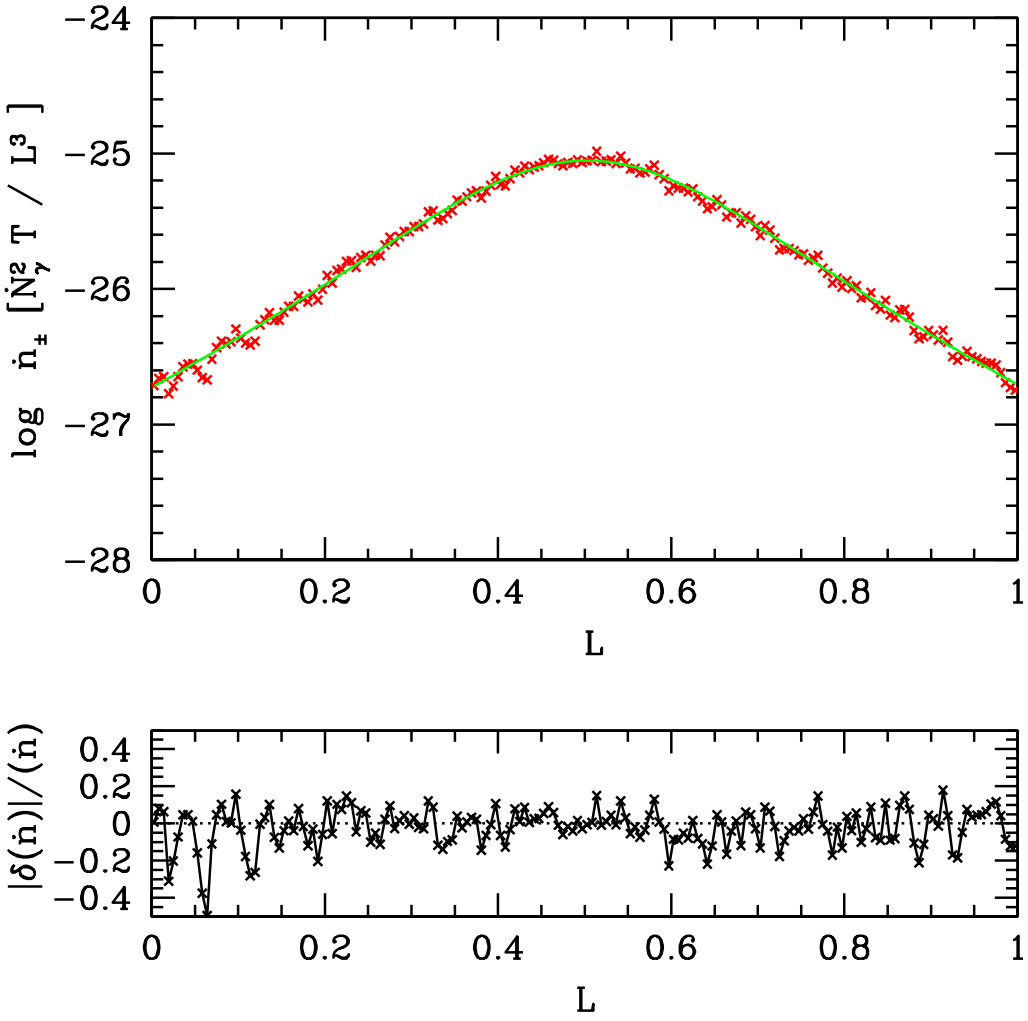

Fig. 3.— Test problem: upper panel: Analytical (green line) and numerical (red points) pair production rates, along the black contour in Figure 2. Lower panel: The fractional difference between analytical and numerical solutions.

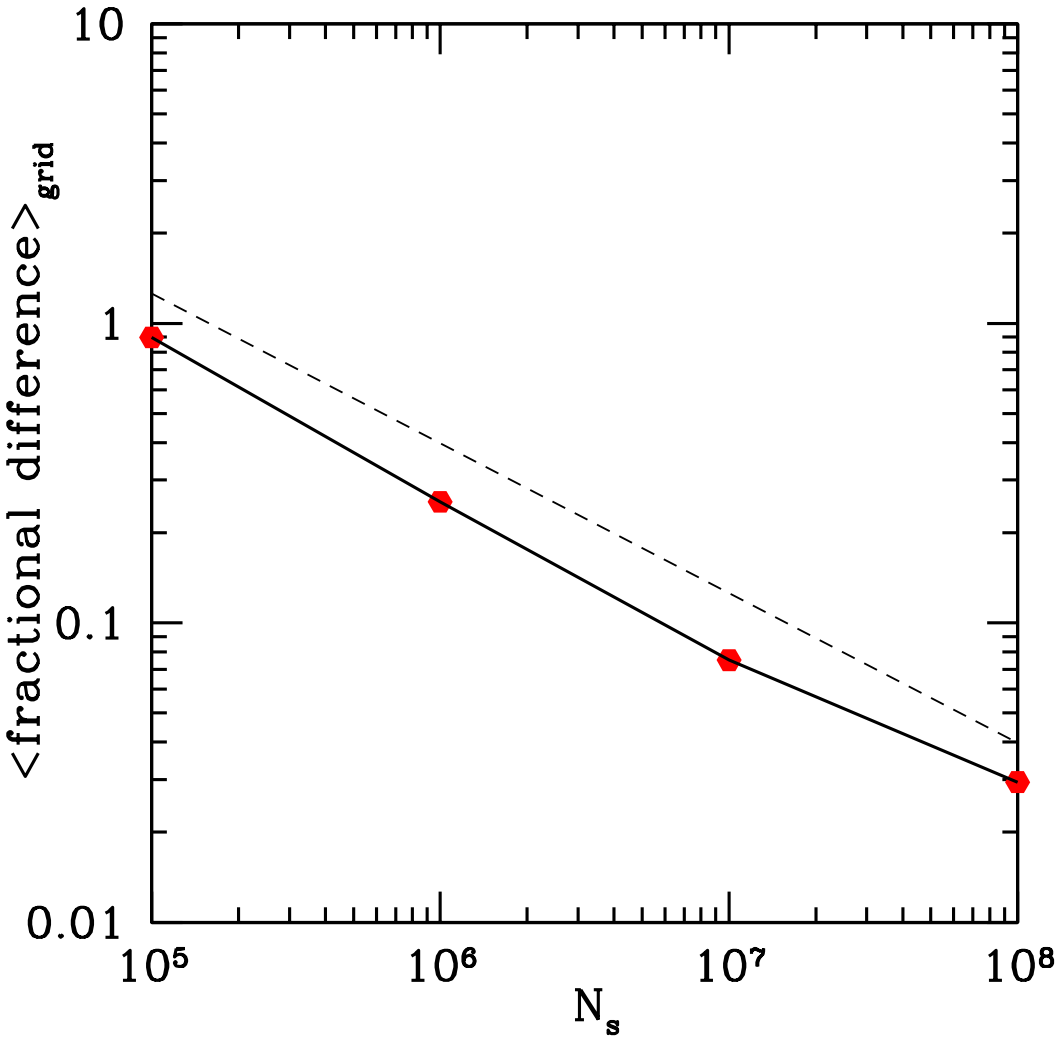

Fig. 4.— Test problem: the grid averaged fractional difference between the numerical and analytical pair production rates as a function of number of photons packets produced by each source N_s. The dashed line is proportional to $N_s^{-1/2}$. For $N_s = 10^7$ the average difference per zone is about 7%, for $N_s = 10^8$ it is on average less than 3%.

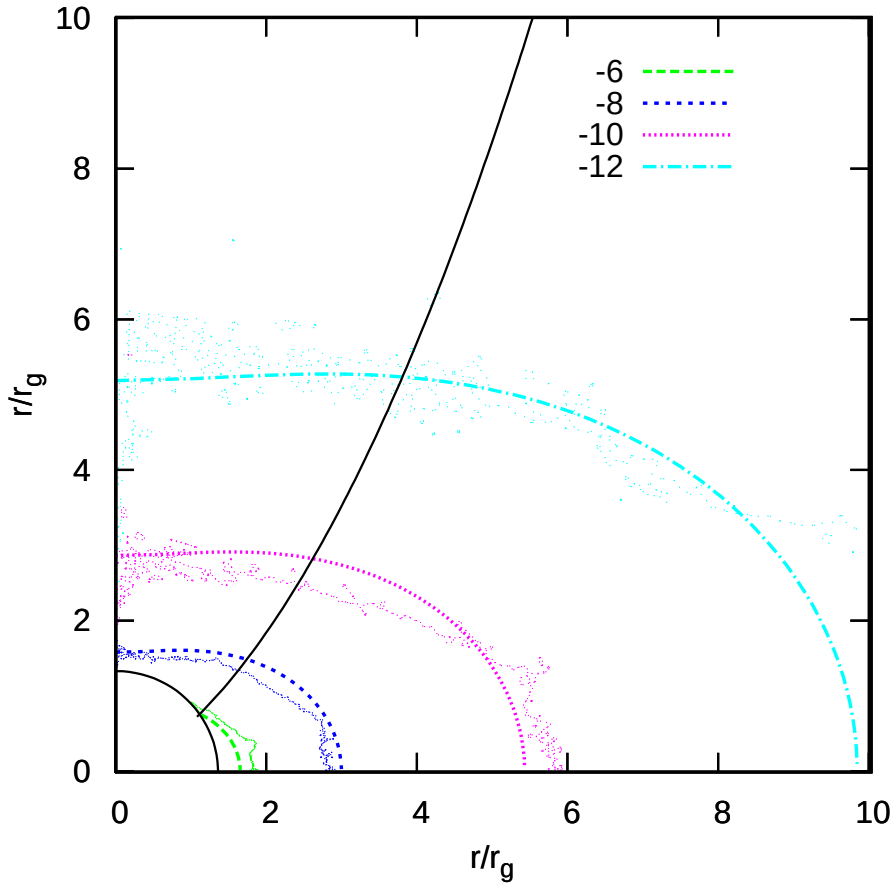

Fig. 5.— Spatial distribution of $\dot{n}_{\pm}$in RIAF model C (points) and the contours of corresponding fitting function given by Equation 26 (lines). The fractional difference between model and data in this case is $< 40\%$. Black contours mark the black hole horizon and the funnel wall.

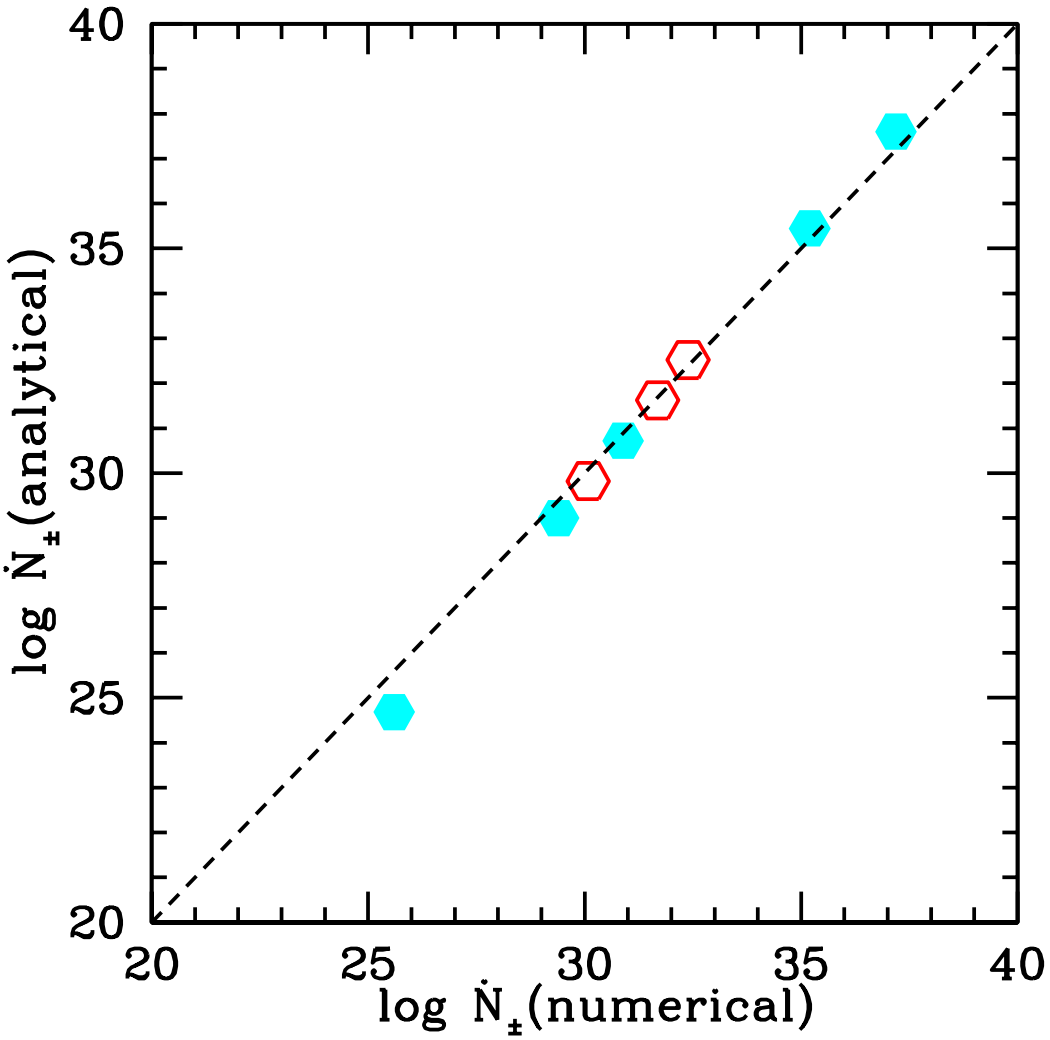

Fig. 6.— Pair production rate dependence on the model parameters. Comparison of the total pair production rate $\dot{N}_{\pm}$ to the fitting formula for models with various mass accretion rates $\dot{m}$ (A-E, blue filled symbols), and black hole masses m (F-H, red open symbols). The $\dot{N}_{\pm}$(analytical) is given by Equation 28.

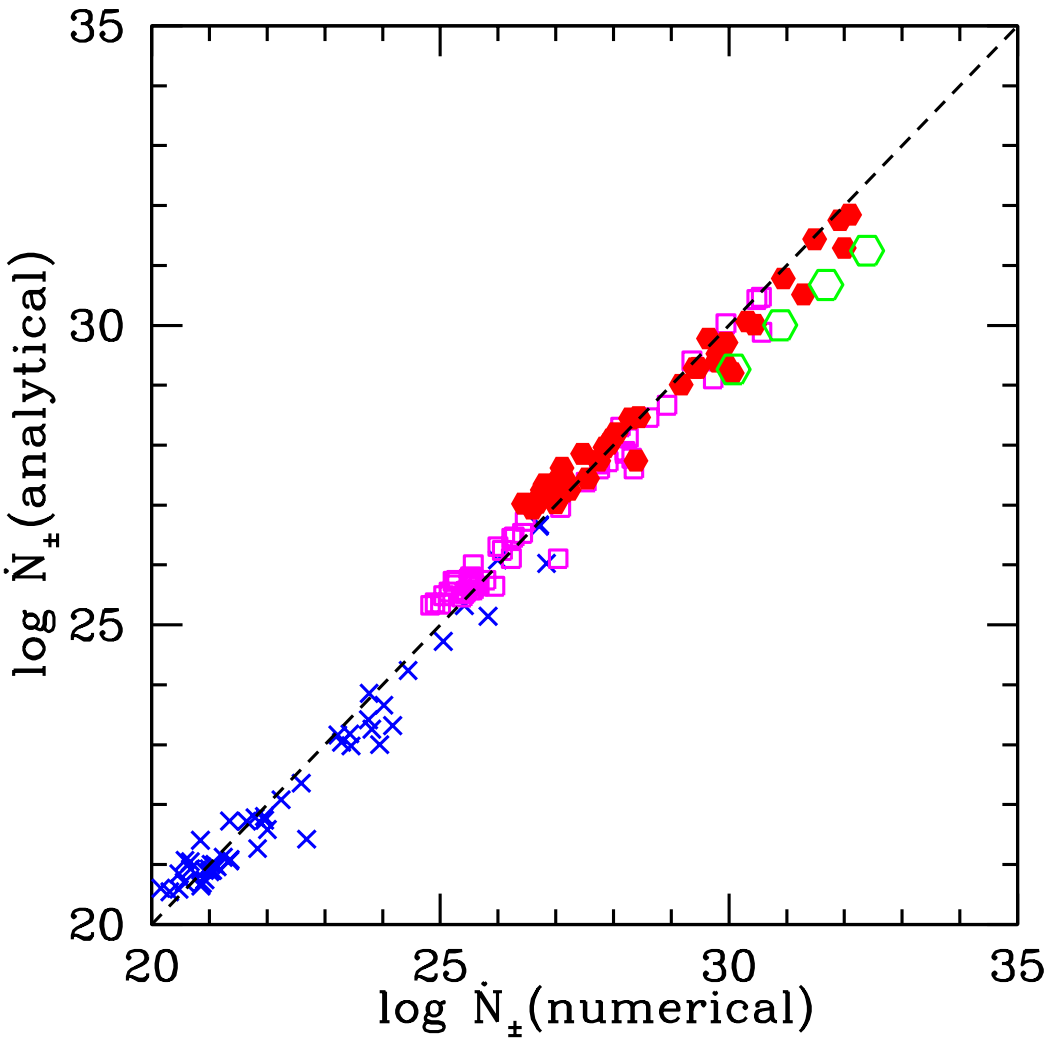

Fig. 7.— Pair production rate dependence on observable parameters. Comparison of the total pair production rate $\dot{N}_{\pm}$ to the fitting formula for models with different X-ray luminosities $(\nu L_{\nu})_{2-10keV}$, X-ray spectral index α_X and masses. Filled circles, open squares, and crosses correspond to different snapshots in models A, B, and C, respectively. Open circles mark time averaged data from models with different masses (F, G, and H). The $\dot{N}_{\pm}$(analytical) is given by Equation 30.

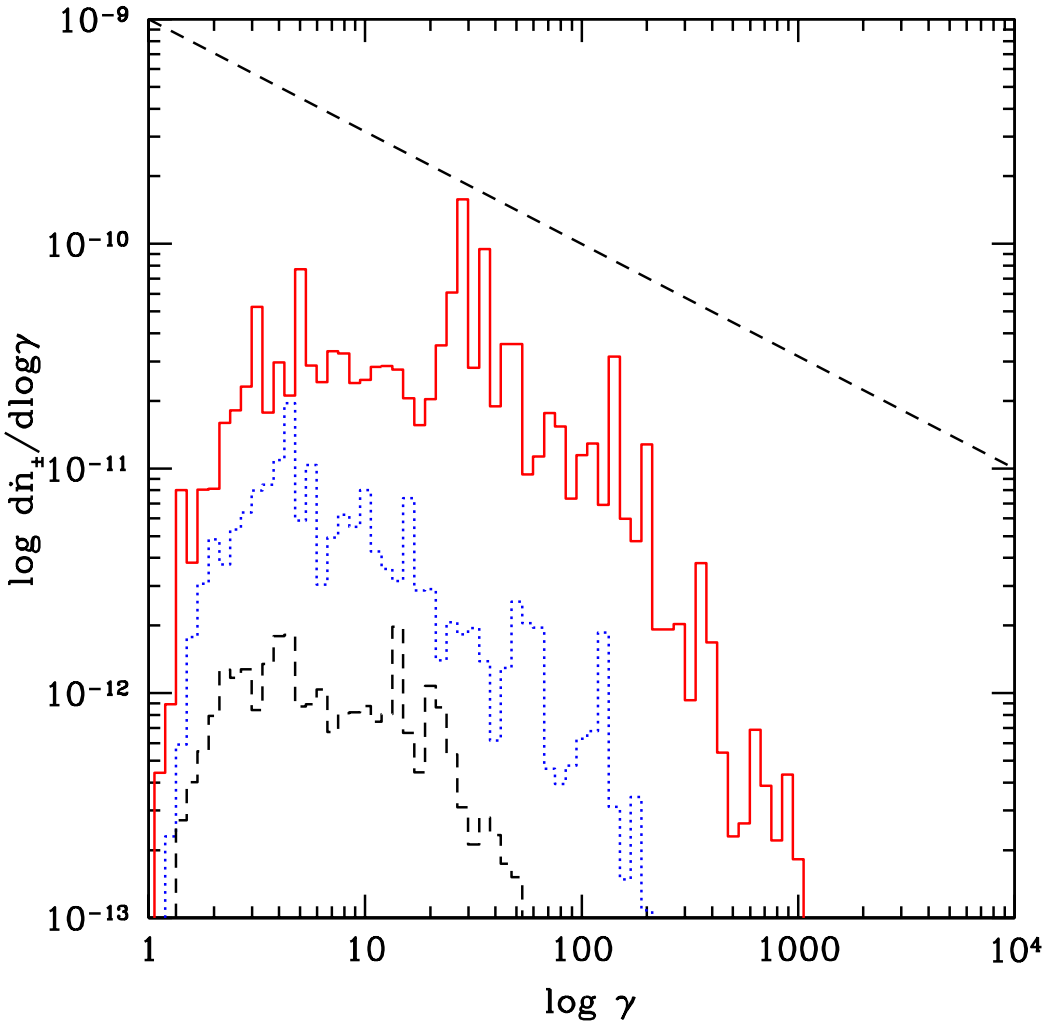

Fig. 8.— The energy distribution of $e^{\pm}$ pairs produced in the magnetized funnel where $\gamma = \gamma_{e^{\pm}[FF]}$ is measured in the plasma frame at different radii (model C).

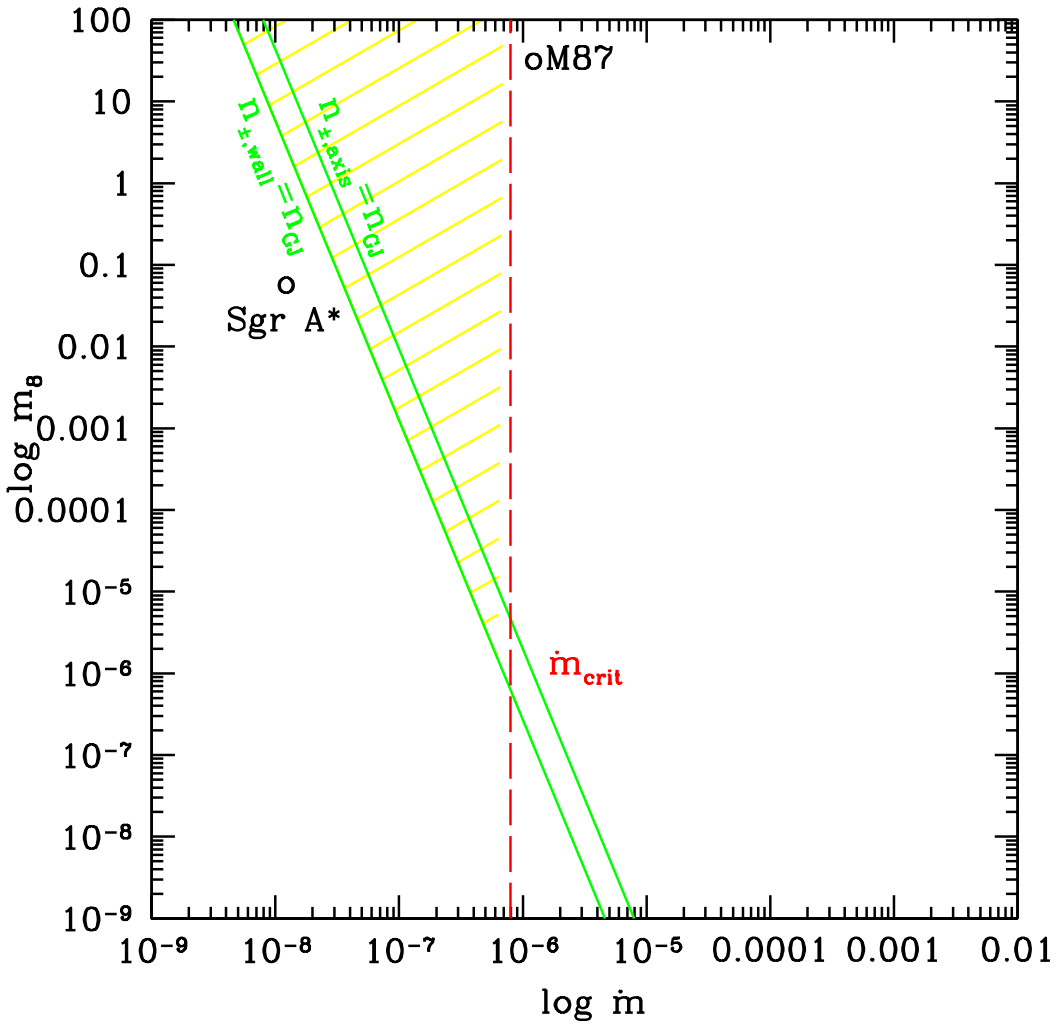

Fig. 9.— Fitting formulas are fully selfconsistent with the model assumptions for m and $\dot{m}$ within the shaded region. Two solid lines mark regions where the n_{GJ} equals to the pair density at the funnel axis and funnel wall. LLGN of interest are marked as open circles.